

A kinetic model for the methane hydrate precipitated from venting gas at cold seep sites at Hydrate Ridge, Cascadia margin, Oregon

Yuncheng Cao,^{1,2} Duofu Chen,^{1,2} and Lawrence M. Cathles³

Received 1 April 2013; revised 12 August 2013; accepted 21 August 2013.

[1] We develop a kinetic model for hydrate crystallization from methane gas venting through shallow sediments at Hydrate Ridge on the Cascadia margin of Oregon that predicts how pore water chlorinity, temperature, and crystallized hydrate evolve after the onset of steady venting. Predictions are compared to observations at Ocean Drilling Program Site 1249. In the preferred model, calculated gas hydrate saturation and chloride concentrations reach those observed at depths less than 20 m below seafloor (bsf) under the southern summit of Hydrate Ridge in ~650 years, and the vertical water flux must be less than 50 kg/m²/yr. Hydrate accumulates more slowly between 20 m bsf and the base of the hydrate stability zone where there is no free gas, accumulating to observed levels of a few volume percent of hydrate in 10⁵ to 10⁶ years, depending on the water flux that is assumed through this zone. This dichotomy means that the presently observed gas venting must have been diverted to this area ~650 years ago, or be episodic and infrequent. If the gas venting for the last 650 years has been as observed today, the latent heat of hydrate precipitation in the upper 20 m of sediments would have caused the temperature to increase ~0.8°C at ~20 m bsf and ~0.2°C at ~100 m bsf. This would have caused a ~5 m rise in the elevation of the base of hydrate stability zone, and decreased the rate of hydrate crystallization from 1.5 kg CH₄/m²/yr 650 years ago to 0.7 kg CH₄/m²/yr today.

Citation: Cao, Y., D. Chen, and L. M. Cathles (2013), A kinetic model for the methane hydrate precipitated from venting gas at cold seep sites at Hydrate Ridge, Cascadia margin, Oregon, *J. Geophys. Res. Solid Earth*, 118, doi:10.1002/jgrb.50351.

1. Introduction

[2] Gas hydrate is an ice-like crystalline mineral in which a rigid cage of water molecules encloses hydrocarbon and nonhydrocarbon gas molecules [Sloan and Koh, 2008]. Hydrate is extremely common over vast areas of the world's shelves and continental slopes, and in arctic permafrost. Estimates of gas stored in hydrates vary between 0.2 and 120 × 10¹⁵ m³ (STP) [Sloan and Koh, 2008], and a significant portion of gas hydrate occurs in reservoirs from which natural gas is technically recoverable [Johnson, 2011]. Gas hydrate also plays a plausible role in submarine geohazards and is an agent in global climate change [Kvenvolden, 1999; Maslin et al., 2010; Reagan and Moridis, 2008;

Reagan et al., 2011; Ruppel, 2011; McConnell et al., 2012]. For these reasons, hydrates have been studied intensively in the last few decades.

[3] The presence of gas hydrate has been inferred in a great number of marine sites worldwide with bottom simulating reflectors (BSR) [Hyndman and Davis, 1992; Sloan and Koh, 2008; Kvenvolden and Lorenson, 2001]. The hydrate stability zone (HSZ) is considered to be a two-phase zone of water and hydrates that lies between the BSR and the seafloor [Chen et al., 2006; Xu and Ruppel, 1999; Zatsepina and Buffett, 1997; Haacke et al., 2007]. Hydrates crystallize from dissolved methane and other dissolved hydrocarbon gases. Pore water movements and aqueous diffusion deliver these gases to the HSZ [Davie and Buffett, 2001, 2003a, 2003b; Xu and Ruppel, 1999; Rempel and Buffett, 1997; Haacke et al., 2008]. In this conception, hydrates are considered to be in thermodynamic equilibrium with the liquid-hydrate (L-H) system in the HSZ [Xu and Ruppel, 1999; Zatsepina and Buffett, 1997, 1998; Xu, 2004; Davie and Buffett, 2003a; He et al., 2006; Bhatnagar et al., 2007]. No free gas is present, and hydrate accumulation is modeled by superimposing heat and mass transport on the L-H thermodynamic equilibrium [Rempel and Buffett, 1997; Xu, 2004; Xu and Ruppel, 1999; Bhatnagar et al., 2007].

[4] In many gas hydrate locations, however, gas bubbles are observed venting from the seafloor [Heeschen et al., 2003; Leifer and MacDonald, 2003; MacDonald et al., 2002; Ivanov et al., 2010; Riedel et al., 2006a, 2006b;

¹CAS Key Laboratory of Marginal Sea Geology, South China Sea Institute of Oceanology, Chinese Academy of Sciences, Guangzhou, China.

²CAS Key Laboratory of Marginal Sea Geology, Guangzhou Institute of Geochemistry, Chinese Academy of Sciences, Guangzhou, China.

³Department of Earth & Atmospheric Sciences, Cornell University, Ithaca, New York, USA.

Corresponding authors: D. Chen, CAS Key Laboratory of Marginal Sea Geology, Guangzhou Institute of Geochemistry, Chinese Academy of Sciences, 511 Kehua Street, Guangzhou 510640, China. (cdf@gig.ac.cn)

L. M. Cathles, Department of Earth & Atmospheric Sciences, Cornell University, 2134 Snee Hall, Ithaca, NY 14853-1504, USA. (lmc19@cornell.edu)

Naudts et al., 2010]. The venting gas is usually associated with mud volcanoes or salt diapirs and domes [*Boetius and Suess*, 2004; *Milkov*, 2000; *Sassen et al.*, 2003; *Whelan et al.*, 2005; *Jerosch et al.*, 2007; *Matsumoto et al.*, 2011]. At the gas venting sites, hydrates are present from the base of the hydrate stability zone (BHSZ) to the seafloor [*Sassen et al.*, 2001; *Chen and Cathles*, 2003, 2005; *Cathles and Chen*, 2004] and outcrop of the seafloor [*MacDonald et al.*, 2003; *Riedel et al.*, 2006a, 2006b; *Ivanov et al.*, 2007; *Simonetti et al.*, 2011; *Torres et al.*, 2011]. Free gas coexists with hydrate and water within the HSZ in these areas [*Bohrmann et al.*, 2002; *Milkov et al.*, 2004]. The hydrate formation in the liquid-hydrate-vapor (L-H-V) system requires consideration of the kinetics of hydrate crystallization from the venting gas [*Chen and Cathles*, 2003, 2005; *Chen et al.*, 2004; *Cathles and Chen*, 2004; *Torres et al.*, 2004a].

[5] Two types of vent gas have been found on the continental shelf and slope that are easily distinguished by their chemical and isotopic composition: thermogenic gas and biogenic gas [*Milkov*, 2005]. Because the structure II hydrates that crystallized from thermogenic gas have a greater affinity for the heavier gases of ethane, propane, and isobutane, the gas that vents from the seafloor has less of the heavier hydrocarbon components than its source. Using the compositional difference between the source gas and venting gas, *Chen and Cathles* [2003] and *Cathles and Chen* [2004] developed a compositional kinetic model for the crystallization and dissolution of hydrate from a thermogenic gas stream and applied it to the Bush Hill of the Gulf of Mexico. *Chen et al.* [2004] suggested that at any instance of time, thermogenic gas vents to the surface through a number of channels at rates ranging from so slow that nearly all the heavier hydrocarbon components are crystallized as hydrate, to rates so fast that only a very small fraction of these components are removed. Furthermore, *Chen and Cathles* [2005] noted that if lateral losses of heat are negligible, heat advection and the latent heat of hydrate crystallization could significantly warm the subsurface, reduce the hydrate stability zone thickness, and decompose previously crystallized hydrate. However, lateral heat losses can be significant enough that these changes in temperature are greatly reduced or eliminated [*Cathles et al.*, 2006].

[6] Hydrate also crystallizes from venting biogenic methane gas at seep sites such as the Haakon Mosby mud volcano, the Black Sea mud volcano, the Malenki mud volcano of Lake Baikal, and seeps on Black Ridge, Hydrate Ridge, and Eel River Basin [*Milkov*, 2005]. The venting biogenic gas is essentially pure methane, and there is thus no compositional difference between the gas venting through the seafloor and the deep source gas. Thus, neither the solubility-temperature model for hydrate formation of the L-H system [*Xu and Ruppel*, 1999; *Zatsepina and Buffett*, 1997] nor the compositional kinetic model for the thermogenic gas venting system [*Chen and Cathles*, 2003] can be used at the biogenic methane gas venting system.

[7] Using the solubility-temperature (depth) equations of the L-H-V system of methane gas, *Torres et al.* [2004a] developed a one-dimensional, nonsteady state kinetic model to simulate the chloride profile and hydrate distribution at the southern summit of Hydrate Ridge. The observed gas hydrate and chloride distributions, which increase abruptly above 20 m below seafloor (bsf), are primarily driven by a decrease

in effective overburden stress in the near surface sediments. They showed that the transport of methane as a free gas phase was necessary to produce the observed high chloride concentrations and showed that methane hydrate precipitates at extremely fast rates ($\sim 1.6 \text{ kg CH}_4/\text{m}^2/\text{yr}$) where gas is present. Massive gas hydrate deposits at the summit were formed in less than 1500 years. The growth of the hydrate deposit was probably arrested by the development of highly saline fluids. The impact of changes in temperature was not considered in their model.

[8] *Liu and Flemings* [2006, 2007] developed a multi-component, multiphase, fluid and heat flow model to describe hydrate formation that accounts for the dynamic effects of hydrate formation on salinity, temperature, pressure, and hydraulic properties. They showed that gas supplied from the free gas zone beneath the hydrate layer depletes water and elevates salinity until the pore water is too saline for further hydrate formation. The pores with elevated salinity provide a channel through which free gas can migrate across the HSZ. They consider that the zone of three-phase stability extends from the seafloor to 50 m bsf at Ocean Drilling Program (ODP) Site 1249 and suggest that there is a zone of three-phase stability from the disrupted BSR to the ridge crest. Their model ignores latent heat which might cause significant temperature changes [e.g., *Chen and Cathles*, 2005].

[9] In this paper, we develop a kinetic model for gas hydrate crystallization from venting biogenic methane that includes heat and ion diffusion. We use this model to interpret the chloride, temperature, and gas hydrate saturation profiles observed at ODP Site 1249 at the southern summit of Hydrate Ridge. Our model shows that the rate of hydrate precipitation is much higher in the L-H-V system than in the underlying L-H system. To reach the observed chloride concentrations, gas hydrate saturations, and temperatures, the massive gas hydrate at the southern summit of Hydrate Ridge must have formed within ~ 650 years, and the water flux must have been less than $\sim 50 \text{ kg}/\text{m}^2/\text{yr}$. Increases in subsurface temperature and salinity caused by hydrate precipitation probably decreased the rate of hydrate crystallization from $1.5 \text{ kg CH}_4/\text{m}^2/\text{yr}$ ~ 650 years ago to $0.7 \text{ kg CH}_4/\text{m}^2/\text{yr}$ today.

2. Geologic Setting and a Conceptual Model

2.1. Geologic Setting

[10] The Hydrate Ridge is a 25 km long and 15 km wide ridge in the Cascadia accretionary complex off the northwestern coast of the United States (Figure 1a). At the southern summit of Hydrate Ridge, the water depth is ~ 800 m, the temperature at the seafloor is 4.31°C , and seawater chloride concentration is $0.558 \text{ mol}/\text{kg}$ [*Trehu et al.*, 2003]. Acoustic images show a gas plume in the water column (Figure 1c) [*Heeschen et al.*, 2003], and gas bubbling has been directly observed [*Boetius and Suess*, 2004; *Torres et al.*, 2002; *Tryon et al.*, 2002]. Deep tow side scan sonar data show a $\sim 300 \times 500$ m area of relatively high acoustic backscatter that indicates seafloor venting [*Johnson et al.*, 2003; *Trehu et al.*, 2004a]. A zone of near-surface, high-amplitude, chaotic reflections, which are correlated with high hydrate content, was observed at the southern summit, and the lateral extent of this seismic pattern is almost exactly coincident with the areas of relatively high acoustic backscatter [*Trehu et al.*,

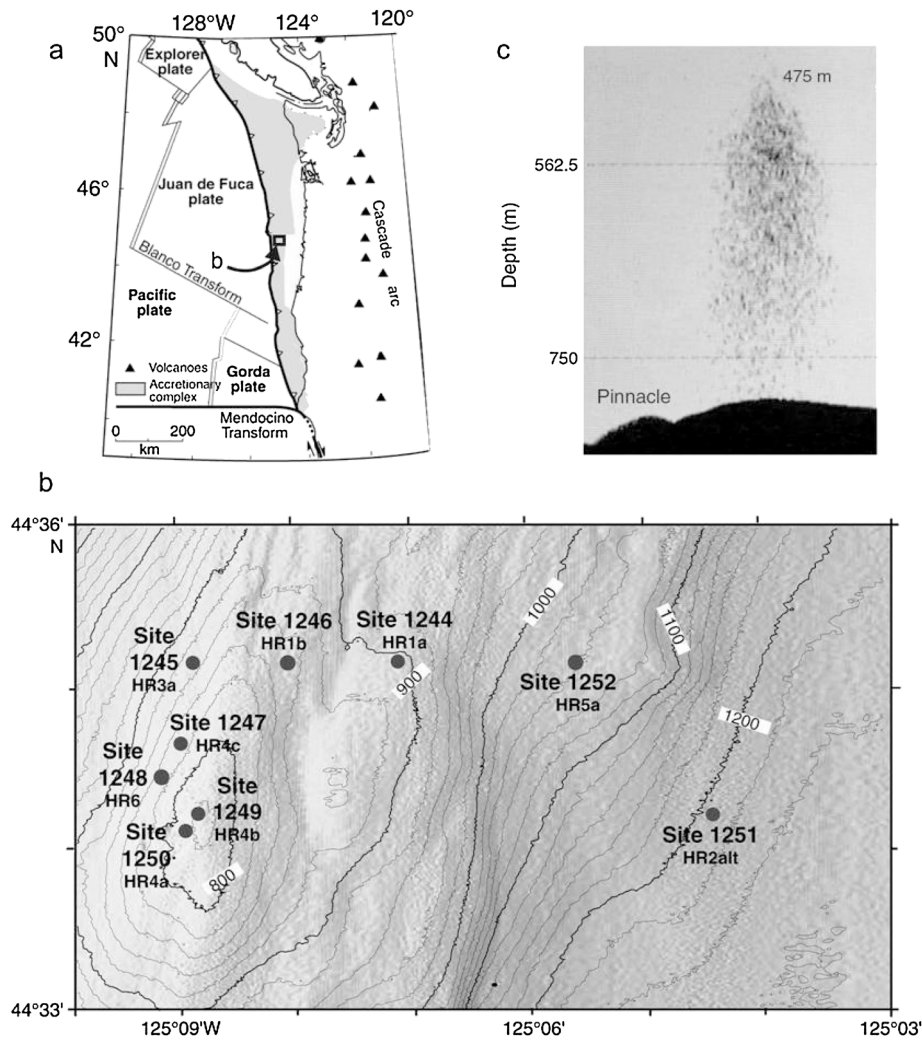


Figure 1. (a) Location and tectonic setting of Hydrate Ridge on the accretionary complex of the Cascadia subduction zone [Trehu *et al.*, 2003]. (b) A bathymetric map of the region of Hydrate Ridge in the box shown in Figure 1a. Leg 204 sites are shown along with their site numbers [Trehu *et al.*, 2003; Clague *et al.*, 2001]. (c) Acoustic image showing the free gas discharging at the southern summit of Hydrate Ridge approximately at the location of ODP Site 1249 [Heeschen *et al.*, 2003].

2004a]. This seismic pattern indicates the depth extent of surface massive hydrate as described by Trehu *et al.* [2003, 2004a].

[11] Free methane gas and high concentrations of hydrate were observed in shallow sediments at the southern summit of Hydrate Ridge [Torres *et al.*, 2002; Trehu *et al.*, 2004a]. Free gas was recovered in a pressure core collected and preserved at in situ pressure from 14 m depth at Site 1249 [Trehu *et al.*, 2003; Milkov *et al.*, 2004]. Heeschen *et al.* [2005] determined that the flux of free gas at the southern summit of Hydrate Ridge was $\sim 1.9 \text{ kg/m}^2/\text{yr}$ across the $1.5 \times 10^5 \text{ m}^2$ area of Hydrate Ridge that contains 30%–40% of pore space hydrate between the seafloor and 20 m bsf as indicated in Figures 3a and 1c. The water flux at the southern summit of Hydrate Ridge is localized and variable. At some discrete gas release points, fluid rapidly escapes from conduits of approximately 1 cm in diameter [Torres *et al.*, 2002]. In the $\sim 100 \text{ m}^2$ seafloor that is covered by thick, dense microbial mats, the water flux is from 100 to 2500 $\text{kg/m}^2/\text{yr}$ [Torres *et al.*, 2002; Tryon *et al.*, 2002]. There are patches of clams

around the microbial mats where the water flux varies from -100 kg/m^2 (downward flow) to $20 \text{ kg/m}^2/\text{yr}$ (upward flow) [Torres *et al.*, 2002; Tryon *et al.*, 2002]. The rest area is chemoherm or sediment covered [Tryon *et al.*, 2002]. Therefore, the amount of water flowing out of the sediments is calculated to be 1×10^4 – $2.5 \times 10^5 \text{ kg/yr}$ for microbial mats and -1.0×10^4 – $2.0 \times 10^3 \text{ kg/yr}$ for clam field (the area of clam field is assumed equal to that of bacterial mat sites according to a surface geological and environmental map of Hydrate Ridge in the work of Tryon *et al.* [2002]). If we spread the current venting from the bacterial mats and clam sites over the area of subsurface hydrate accumulation, the average present-day water flux for the whole area ($1.5 \times 10^5 \text{ m}^2$) of the southern summit of Hydrate Ridge is ~ 0 – $2 \text{ kg/m}^2/\text{yr}$.

[12] Hydrate was recovered from the above 20 m bsf at Site 1249 and by TV-guided grab sampling at the southern summit of Hydrate Ridge [Boetius and Suess, 2004; Suess *et al.*, 1999; Torres *et al.*, 2002; Trehu *et al.*, 2003]. Pressure cores from Site 1249 at 8 m bsf and 14 m bsf, respectively, had a hydrate

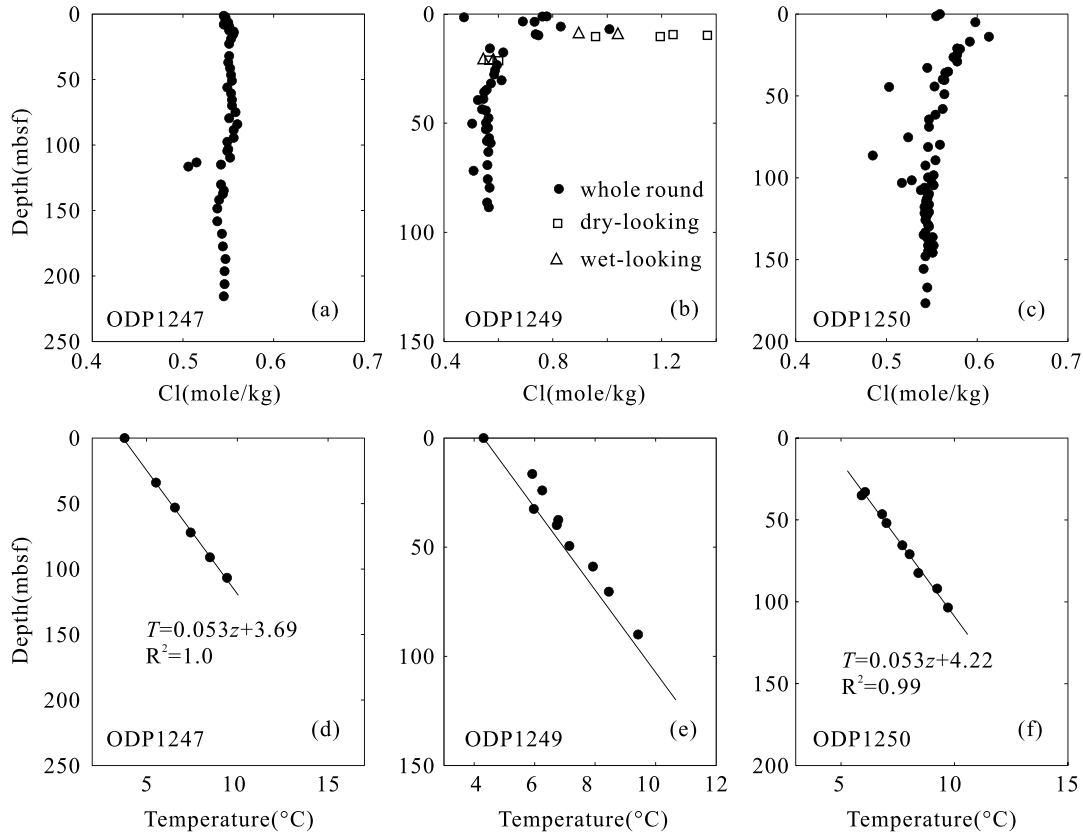


Figure 2. Chloride concentrations and temperature at ODP Site 1247, ODP Site 1249, and ODP Site 1250 [Trehu *et al.*, 2003]. (a) The measured chloride concentrations are close to seawater values at ODP Site 1247. (b) Chloride concentrations show very high values above ~ 20 m bsf of ODP Site 1249. Chloride concentrations measured from whole round samples (cycle) vary from 0.70 to 1.08 mol/kg above ~ 20 m bsf but give way to seawater value below 20 m bsf. The square data points indicate dry-looking samples which show very little gas hydrate dissociation, and the chloride of these dry-looking samples vary from 0.95 to 1.37 mol/kg above 20 m bsf, which is higher than the chloride content of the whole round samples and wet-looking samples that are collected in areas where sediment is liquefied from gas hydrate dissociation (triangles). (c) The chloride concentrations measured at ODP Site 1250 are higher than seawater value at shallow depth, of which the highest value is 0.613 mol/kg. (d) The temperatures measured at ODP Site 1247 define straight line very well, from which the temperature gradient of $0.053^{\circ}\text{C}/\text{m}$ is derived. (e) Black dots indicate measured temperatures at ODP Site 1249. Here the temperature measured by advanced piston corer temperature (APCT) tool has been revised through the inversion for best fit thermal conductivity and in situ temperature and added 0.51°C to temperature derived from APCT 11 for the calibration correction (detail described in Trehu *et al.* [2003]). The measured temperatures show positive anomalies compared to the temperature profile (solid line) defined by the seafloor temperature at ODP Site 1249 and the regional thermal gradient of $0.053^{\circ}\text{C}/\text{m}$. (f) The temperatures display approximately linear profile at ODP Site 1250.

saturation of $\sim 45\%$ (volume fraction of the pore space) [Trehu *et al.*, 2003; Milkov *et al.*, 2004]. However, this hydrate saturation was considered to be an overestimate, and 30% – 40% is a more reasonable estimate for the average gas hydrate content at the southern summit of Hydrate Ridge [Trehu *et al.*, 2004a], even though the gas hydrate saturation may occupy more than 90% of the pore space across some centimeter-scale intervals [Trehu *et al.*, 2003; Milkov *et al.*, 2004]. Pore water samples were recovered from whole (round) cores, and the chloride concentrations at above 20 m bsf are between 0.7 and 1.008 mol/kg [Trehu *et al.*, 2003; Torres *et al.*, 2004b]. In addition, some sediment samples retained their original structure (dry-looking samples), whereas some sediment samples had a “soupy” appearance (wet-looking samples).

Dry-looking samples may reflect high in situ chloride concentration, which ranges from 0.9 to 1.37 mol/kg above 20 m bsf [Trehu *et al.*, 2003; Torres *et al.*, 2004b].

[13] Below ~ 20 m bsf, gas hydrate saturation is only $\sim 2\%$ – 4% , and chloride values approach seawater concentration [Trehu *et al.*, 2004a]. At Site 1249, pore water chlorinity in the dry-looking core samples at 21.12 and 21.38 m bsf are 0.566 and 0.601 mol/kg [Trehu *et al.*, 2003], respectively, which are very close to normal seawater values and very different from the chlorinity concentrations above ~ 20 m bsf.

[14] In situ temperatures measured at ODP Site 1249 at the southern summit of Hydrate Ridge are shown in Figure 2e. We believe that this temperature has been increased by heat advection and the latent heat of hydrate crystallization. There is no

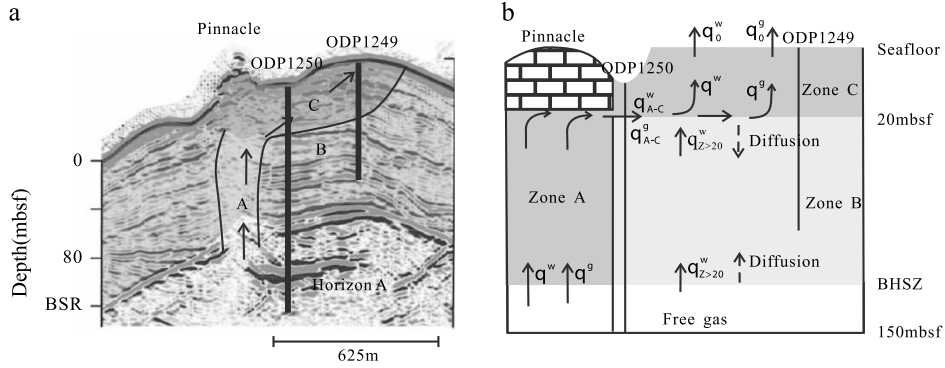


Figure 3. (a) A seismic cross section at southern Hydrate Ridge [Trehu *et al.*, 2003] shows a BSR at the bottom of a gas hydrate zone at ~ 115 m bsf. Gas appears to flow upward through Zone A and could be diverted across Zone C by the near-surface low-permeability carbonate layers at Pinnacle (location of ODP Site 1250). The gas hydrate saturation in Zone C is 30%–40%, and 2%–4% in Zone B [Trehu *et al.*, 2004a]. In our modeling, we assume that gas is present in Zones A and C (both are L-H-V systems), but gas is absent in Zone B which is an L-H system. (b) A schematic diagram of the flow of gas and water that we model. Free gas and water flow upward from Horizon A to 20 m bsf and are then diverted laterally along the 20 m bsf horizon where they leak upward into Zone C [Milkov and Xu, 2005; Liu and Flemings, 2006]. Methane dissolves in pore water and diffuses downward into the hydrate stability zone (HSZ) from the bottom ~ 20 m bsf.

active fluid venting 800 m northwest of Hydrate Ridge at ODP Site 1247 (Figure 1). The gas hydrate saturation there is 2%–4%, and the chloride concentration is very close to the seawater value. Therefore, the thermal gradient of $0.053^\circ\text{C}/\text{m}$ (Figure 2d) estimated from the in situ temperature at this site is probably much closer to the background thermal gradient. The temperature (solid line in Figure 2e) defined by the seafloor temperature at ODP Site 1249 and the background thermal gradient of $0.053^\circ\text{C}/\text{m}$ are significantly lower than the measured values at ODP Site 1249 (Figure 2e). This suggests that fluids moving upward at ODP Site 1249 have increased the subsurface temperature at the southern summit of Hydrate Ridge.

2.2. Conceptual Model

[15] Milkov and Xu [2005] and Liu and Flemings [2006] suggested that gas and water from Horizon A flow vertically beneath the Pinnacle near ODP Site 1250 and are then diverted laterally toward the South Ridge summit near ODP Site 1249 (see Figures 1c and 3a). We simplify this suggestion as shown in Figure 3b by assuming that free gas and water vent flow vertically in Zone A to 20 m bsf and then move laterally at a depth of 20 m bsf (the boundary between Zones B and C) while at the same time leaking vertically through Zone C. There is no free gas in Zone B, but there is a vertical flow of water. We allow for biogenic methane production in Zone B and Zone C.

[16] Our method is to determine the water and gas flux coming from Zone A by extrapolating downward to 20 m bsf from the water and gas fluxes observed on the seafloor. We set the surface gas flux at the $1.9\text{ kg}/\text{m}^2/\text{yr}$ rate determined by Heeschen *et al.* [2005] and determine the surface water flux that is compatible with observed temperature and chloride profiles through modeling. The temperature and chloride concentration of the fluids that migrate from Zone A to Zone C at 20 m bsf are considered to be those measured at ODP Site 1250. We set the water flux at the base of the

hydrate stability zone (Zone B) to $0.5\text{ kg}/\text{m}^2/\text{yr}$, according to the water flux estimated for the seaward-most 18 km of Cascadia accretionary prism by Carson and Westbrook [1995]. We set the biogenic methane production in Zone C and Zone B at $6.8 \times 10^{-8}\text{ kg}/\text{m}^3/\text{yr}$ based on Colwell *et al.* [2008]. The hydrate accumulation, water salinities, and temperature change in Zones B and C can be computed as a function of time for these fluxes, considering also the diffusion of dissolved methane, and the comparison of the calculated profiles to observations constrains (for a reasonable range of water fluxes in Zone C) the length of time that gas and water flow has been diverted along the 20 m bsf horizon.

3. Numerical Model

[17] The rate of methane, water consumption, and heat release are proportional to the hydrate growth rate. The rate of methane consumption due to hydrate crystallization is determined by a first order rate equation [Chen and Cathles, 2003]:

$$R_g = -k \cdot \Delta X \cdot \exp\left(\frac{E}{R} \left(\frac{1}{T^*} - \frac{1}{T}\right)\right) \cdot \phi \cdot (1 - S_h), \quad (1)$$

where R_g ($\text{kg}/\text{m}^3/\text{yr}$) is the rate of methane consumption per unit volume sediment, k ($\text{kg}^2/\text{m}^3/\text{yr}/\text{mol}$) is the rate constant, ΔX (mol/kg) is the driving force calculated from difference between the local dissolved methane concentration and the methane concentration that would be in equilibrium with hydrate as described below, E is the activation energy of the reaction, R is the gas constant (we take $E/R = 10,000\text{ K}$), T^* is an arbitrary reference temperature (taken to be 273.15 K), T (K) is the temperature (converted to degrees Celsius below), ϕ is the porosity of the sediment, and S_h is hydrate saturation (volume fraction of the pore space filled with gas hydrate). The term of $\phi \cdot (1 - S_h)$ is added to the expression of Chen and Cathles [2003] so that the reaction

stops when the pore space is filled. Kinetic dependence on pore space indicates that the presence of more gas and water per unit volume of sediment will support a higher hydrate crystallization rate.

[18] In the L-H-V system above 20 m bsf (Zone C), the driving force is determined by the deviation from the three-phase equilibrium conditions for the gas hydrate crystallization process [Englezos *et al.*, 1987a, 1987b; Clarke and Bishnoi, 2000, 2001; Giraldo *et al.*, 2013] defined by $\Delta X = X_m^{L-V} - X_m^{L-H-V}$, where X_m^{L-V} (mol/kg) is the methane concentration in equilibrium with methane gas (the L-V system) under local temperature and pressure, calculated as described by Duan *et al.* [1992]; X_m^{L-H-V} (mol/kg) is the methane solubility in the L-H-V system at the three-phase equilibrium pressure corresponding to the local temperature, which is calculated by using a data-fitting empirical equation developed by Anderson [2004] as described by Chen *et al.* [2006].

[19] In the L-H system below ~20 m bsf (Zone B), there is no free gas, and the driving force is determined by the deviation from methane solubility in equilibrium with hydrate in the L-H system [Davie and Buffett, 2003a]. Thus, $\Delta X = X_m - X_m^{L-H}$, where X_m (mol/kg) is the methane concentration that results from methane diffusion, advection of pore water with dissolved methane, methane biogenic production, and hydrate formation as described in equation (10) below, and X_m^{L-H} (mol/kg) is methane solubility in equilibrium with hydrate in the L-H system as described by Davie *et al.* [2004].

[20] The hydrate growth rate is related to the rate of methane consumption:

$$A_h = -\frac{M_h}{n_h \cdot M_g} R_g, \quad (2)$$

where A_h (kg/m³/yr) is the mass of hydrate that forms per unit volume of sediment per year, M_h and M_g (kg/mol) are the hydrate and methane molecular weights (taken $M_h = 0.1223$ kg/mol [Torres *et al.*, 2004b] and $M_g = 0.016$ kg/mol), and n_h is the moles of CH₄ per mole of hydrate and $n_h = 1$.

[21] The rate of water consumption, A_w (kg/m³/yr), and the rate of heat release, A_T (J/m³/yr), are related to the rate of hydrate formation:

$$A_w = \frac{M_h - n_h \cdot M_g}{n_h \cdot M_g} R_g, \quad (3)$$

$$A_T = A_h \cdot H = -\frac{M_h}{n_h \cdot M_g} R_g \cdot H, \quad (4)$$

where H is the latent heat of hydrate crystallization and dissolution ($H = 416,000$ J/kg; Rueff *et al.* [1988]).

[22] Methane precipitates as hydrate (R_g), which depletes methane, but methane can also be generated by biogenic reactions, so the total source term for methane, A_g (kg/m³/yr), is

$$A_g = R_g + B_g, \quad (5)$$

where B_g (kg/m³/yr) is the rate of biogenic methane production ($< 6.8 \times 10^{-8}$ kg/m³/yr; Colwell *et al.* [2008]).

[23] The porosity is assumed to decrease exponentially with depth:

$$\phi = \phi_f + (\phi_0 - \phi_f) \cdot \exp(-\alpha \cdot z). \quad (6)$$

[24] Here ϕ_f is the porosity at infinite depth, ϕ_0 is the porosity at zero depth, α (m⁻¹) is an attenuation coefficient, and z (m bsf) is sediment depth [Torres *et al.*, 2004b]. The sediment pores are filled with gas, hydrate, and water, so $S_w + S_g + S_h = 1$. Here S_g and S_w represent gas and water saturation, which are volume fractions of the pore space filled with gas and water, respectively. Changes in hydrate saturation can be described by the following equation:

$$\phi \frac{\partial S_h}{\partial t} = \frac{A_h}{\rho_h}, \quad (7)$$

where ρ_h (kg/m³) is density of hydrate, which is taken to be 912 kg/m³ [Sloan and Koh, 2008], and t (year) is the time.

[25] Above 20 m bsf, we assume methane transported as free gas only, and we ignore the diffusion of dissolved methane because it is very small compared with that transported as free gas. When methane gas migrates from deep sources along conduits toward the seafloor, methane gas partially forms gas hydrate and partially fills the pore space of the sediments, and the remaining methane gas emanates from the seafloor. Milkov *et al.* [2004] estimated the pore space at 14 m bsf at Site 1249 had 40% gas hydrate and 10% free gas, showing that the gas hydrate contains much more methane than the methane gas which fills the pore space. Therefore, we can ignore the amount of methane gas that fills the pore space and only consider the methane that forms gas hydrate and emanates from seafloor. In our calculations, we assume the gas pore fraction is constant ($S_g = 0.1$) in the Zone C ($z = 0-20$ m bsf) and that $S_g = 0$ in Zone B ($z > 20$ m bsf). We take q^g and q^w to be positive upward. The gas fluxes at any location are calculated from the gas flux, q_o^g (kg/m²/yr), at the seafloor ($z = 0$ m bsf):

$$q^g = \begin{cases} q_o^g - \int_0^z A_g dz & (z \leq 20) \\ 0 & (z > 20) \end{cases}, \quad (8)$$

[26] Here $q_o^g = 1.9$ kg/m²/yr, the average observed gas flux at the southern summit of Hydrate Ridge as determined by Heeschen *et al.* [2005].

[27] Due to the density difference between water and hydrate, there is a volume change of hydrate formation which produces a divergence of water flow. However, the density difference is relatively small and water flux can be assumed to be a constant value [Rempel and Buffett, 1997]. The water flux is calculated as

$$q^w = \begin{cases} q_o^w & (z \leq 20) \\ q_{z>20}^w & (z > 20) \end{cases}, \quad (9)$$

where q_o^w (kg/m²/yr) is constrained by the observed chloride, hydrate, and temperature profiles observed at ODP Site 1249, as discussed in section 4 below.

Table 1. Parameters Used in Calculation at ODP Site 1249 at the Southern Summit of Hydrate Ridge

Parameters	Value	References
Water depth (m)	778	<i>Trehu et al., 2003</i>
l , length of system, depth at Horizon A (m bsf)	150	<i>Trehu et al., 2004b, 2003</i>
d , depth of vent hydrate system (m bsf)	20	
α , attenuation coefficient (m^{-1})	1.4×10^{-6}	<i>Torres et al., 2004b</i>
ϕ_0 , porosity at seafloor sediment	0.687	<i>Torres et al., 2004b</i>
ϕ_∞ , porosity at infinite depth	0.542	<i>Torres et al., 2004b</i>
q_0^g , gas flux ($\text{kg}/\text{m}^2/\text{yr}$) across 10^5 m^2 area	1.9	<i>Heeschen et al., 2005</i>
q_0^w , water flux ($\text{kg}/\text{m}^2/\text{yr}$) across 10^5 m^2 area	0–2	<i>Torres et al., 2002; Tryon et al., 2002</i>
B_g , rate of biogenic methane production ($\text{kg}/\text{m}^3/\text{yr}$)	6.8×10^{-8}	<i>Colwell et al., 2008</i>
T_0 , temperature at seafloor ($^\circ\text{C}$)	4.31	<i>Trehu et al., 2003</i>
G_i thermal gradient at ODP Site 1247 ($^\circ\text{C}/\text{m}$)	0.053	<i>Trehu et al., 2003</i>
X_{cl}^0 , seawater chloride concentration (mol/kg)	0.558	<i>Torres et al., 2004b</i>

[28] There are discontinuities of methane gas flux and water flux at 20 m bsf because of the lateral inflow of gas and water from Zone A to Zone C. The lateral influx of gas (q_{A-C}^g [$\text{kg}/\text{m}^2/\text{yr}$]) and water (q_{A-C}^w [$\text{kg}/\text{m}^2/\text{yr}$]) at 20 m bsf are given by $q_{A-C}^g = q_{z=20}^g$ and $q_{A-C}^w = q_{z=20}^w - q_{z>20}^w$, respectively. Below 20 m bsf, there is no free gas and $q_{z>20}^g = 0 \text{ kg}/\text{m}^2/\text{yr}$. Based on the long-term total pore volume loss, the regional rate of water expulsion from the seaward-most 18 km of the Cascadia accretionary prism is estimated to be between ~ 0.9 and $0.1 \text{ kg}/\text{m}^2/\text{yr}$ [*Carson and Westbrook, 1995*]. We set the water flux $q_{z>20}^w$ ($\text{kg}/\text{m}^2/\text{yr}$) = $0.5 \text{ kg}/\text{m}^2/\text{yr}$ in Zone B (below 20 m bsf).

[29] Methane dissolved in pore water is transported by diffusion and advection as described by the following equation:

$$\frac{\partial}{\partial t} (S_w \cdot \phi \cdot \rho_w \cdot X_m) = \frac{\partial}{\partial z} \left(S_w \cdot \phi \cdot \frac{D_m}{\theta^2} \cdot \frac{\partial (\rho_w \cdot X_m)}{\partial z} \right) + \frac{\partial}{\partial z} (q^w \cdot X_m) + A_g / M_g. \quad (10)$$

[30] Here ρ_w (kg/m^3) is water density and we set $\rho_w = 1030 \text{ kg}/\text{m}^3$ [*Torres et al., 2004b*]. D_m (m^2/yr) is diffusion coefficient of methane in water (taken $0.03 \text{ m}^2/\text{yr}$; *Davie and Buffett [2001]*), and θ is tortuosity which is related to water saturation by Archie's law: $\theta^2 = (S_w \cdot \phi)^{-1}$ [*Torres et al., 2004b*].

[31] Changes in the chloride concentration of pore water, X_{cl} (mol/kg), are constrained by the chloride mass balance equation:

$$\frac{\partial}{\partial t} (\rho_w \cdot S_w \cdot \phi \cdot X_{cl}) = \frac{\partial}{\partial z} \left(S_w \cdot \phi \cdot \frac{D_{cl}}{\theta^2} \cdot \frac{\partial (\rho_w \cdot X_{cl})}{\partial z} \right) + \frac{\partial}{\partial z} (q^w \cdot X_{cl}), \quad (11)$$

Where D_{cl} (m^2/yr) is diffusion coefficient of chloride in water (taken $0.03 \text{ m}^2/\text{yr}$; *Davie and Buffett [2001]*).

[32] Finally, temperature changes are constrained by heat balance:

$$\rho_m c_m \cdot \frac{\partial T}{\partial t} = \frac{\partial}{\partial z} \left(\lambda \cdot \frac{\partial T}{\partial z} \right) + (c_g \cdot q^g + c_w \cdot q^w) \cdot \frac{\partial T}{\partial z} + A_T, \quad (12)$$

where λ ($\text{J}/\text{m}^\circ\text{C}/\text{yr}$) is the thermal conductivity, which we set at $3.15 \times 10^7 \text{ J}/\text{m}^\circ\text{C}/\text{yr}$ [*Trehu et al., 2003*], $\rho_m c_m$ ($\text{J}/\text{m}^3/^\circ\text{C}$) is the heat capacity of porous media, c_g and c_w ($\text{J}/\text{kg}/^\circ\text{C}$) are the heat capacity of gas and water [$c_g = 3000 \text{ J}/\text{kg}/^\circ\text{C}$, $c_w = 4200 \text{ J}/\text{kg}/^\circ\text{C}$, *Chen and Cathles, 2005*], and

$$\rho_m c_m \approx c_w \cdot S_w \cdot \rho_w \cdot \phi + c_h \cdot \rho_h \cdot S_h \cdot \phi + c_s \cdot \rho_s \cdot (1 - \phi), \quad (13)$$

where c_s ($\text{J}/\text{kg}/^\circ\text{C}$) and c_h ($\text{J}/\text{kg}/^\circ\text{C}$) are the heat capacities of sediment and hydrate ($c_s = 2200 \text{ J}/\text{kg}/^\circ\text{C}$, $c_h = 2080 \text{ J}/\text{kg}/^\circ\text{C}$; *Davie and Buffett [2001]*).

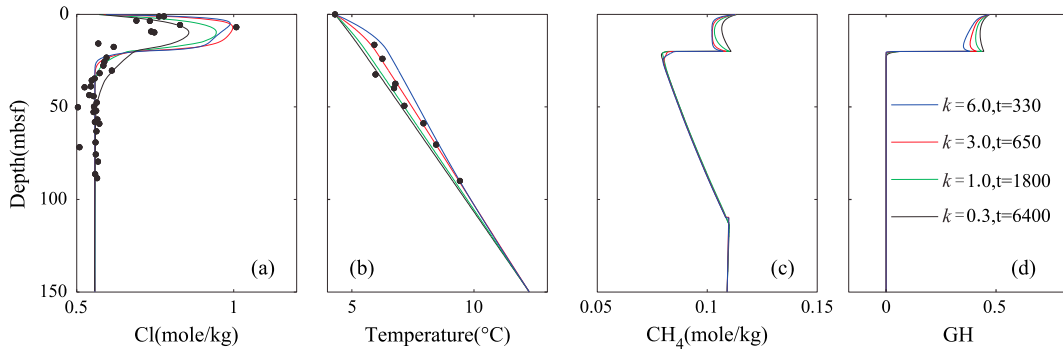


Figure 4. Measurements at ODP Site 1249 from *Trehu et al. [2003]* compared to calculated values. (a, b, c, and d) Calculated chloride concentration, temperature, methane concentration, and gas hydrate saturation profiles for hydrate formation rate constant $k = 0.3, 1.0, 3.0,$ and $6.0 \text{ kg}^2/\text{m}^3/\text{yr}/\text{mol}$ when gas hydrate saturation at 0–20 m bsf reaches the measured value of $\sim 40\%$. In all calculations, the seafloor water flux $q_0^w = 0.5 \text{ kg}/\text{m}^2/\text{yr}$. At $k = 3.0 \text{ kg}^2/\text{m}^3/\text{yr}/\text{mol}$, the calculated temperature profile closely fits the measured values.

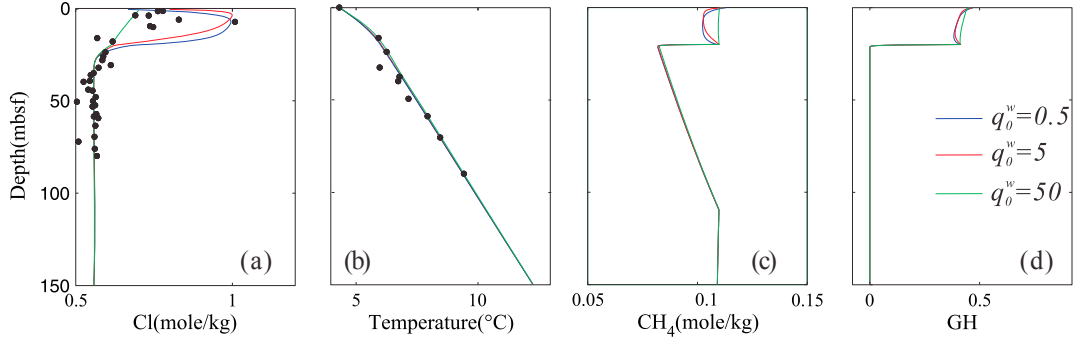


Figure 5. (a) Chloride concentration, (b) temperature, (c) methane concentration, and (d) gas hydrate saturation profiles at ODP Site 1249 calculated for $k = 3 \text{ kg}^2/\text{m}^3/\text{yr}/\text{mol}$ and $t = 650$ years for $q_0^w = 0.5, 5,$ and $50 \text{ kg}/\text{m}^2/\text{yr}$ are compared to measurements by *Trehu et al.* [2003]. The calculated chloride concentration profiles fit the measured data when $q_0^w = 0.5,$ and $5 \text{ kg}/\text{m}^2/\text{yr}$ but are lower than the measured value at $q_0^w = 50 \text{ kg}/\text{m}^2/\text{yr}$. The similarity of the temperature profiles for $q_0^w = 0.5, 5,$ and $50 \text{ kg}/\text{m}^2/\text{yr}$ indicates that the latent heat of hydrate precipitation is the main factor that increases the temperature.

[33] As illustrated in Figure 3b, these equations are solved subject to the following initial and boundary conditions:

[34] 1. The gas hydrate saturation is set to 0 at 0–150 m bsf at $t = 0$ ($S_h(z, t = 0) = 0$);

[35] 2. The initial methane concentration between 20 m bsf and the BHSZ is assumed to the methane solubility in the L-H system ($X_m(z, 0) = X_m^{L-H}(z, 0)$). There is a free gas at 20 m bsf and at the BHSZ, and the methane concentration at the boundaries of Zone B are the dissolved methane concentrations which are in equilibrium with free gas:

$$\begin{aligned} X_m(z = 20, t) &= X_m^{L-V}(z = 20, t), X_m(z = \text{BHSZ}, t) \\ &= X_m^{L-V}(z = \text{BHSZ}, t). \end{aligned} \quad (14)$$

At $t = 0$, the calculated methane concentration is 0.113 mol/kg at 20 m bsf and 0.110 mol/kg at the BHSZ. Since the temperature at the boundaries can vary with time as heat is released by hydrate crystallization, these boundary conditions are a function of time.

[36] 3. We assume initial temperature, $T(z, 0) = T_0 + z \cdot G_i$, where $G_i = 0.053^\circ\text{C}/\text{m}$ as measured at ODP Site 1247 [Trehu et al., 2003]. We assume the surface temperature, T_0 , is constant at 4.31°C as measured at ODP Site 1249 [Trehu et al., 2003]. We assume that the temperature at 150 m bsf, which is the depth of Horizon A at the southern summit of Hydrate Ridge [Trehu et al., 2004b], is constant and equal to 12.3°C (which is the temperature predicted by a surface temperature of 4.31°C and a temperature gradient of $0.053^\circ\text{C}/\text{m}$, see Figure 2e):

$$T(z = 0, t) = 4.31, T(z = l, t) = 12.3. \quad (15)$$

[37] 4. Similarly we assume the initial and boundary conditions for chlorinity:

$$X_{cl}(z, 0) = X_{cl}^0, \quad (16)$$

$$X_{cl}(z = 0, t) = X_{cl}^0, X_{cl}(z = l, t) = X_{cl}^0, \quad (17)$$

where the surface chlorinity $X_{cl}^0 = 0.558 \text{ mol}/\text{kg}$ is the measurement at ODP Site 1249 bottom water [Trehu et al., 2003; Torres et al., 2004b].

[38] 5. At 20 m bsf, water and gas migrate from Zone A to Zone C, and equations (11) and (12) cannot be used to calculate the chloride concentration and temperature at this depth. Migration of water and gas from Zone A to Zone C is needed to be considered in calculation of temperature and chloride concentration at 20 m bsf:

$$\rho_m c_m \cdot \frac{\partial T}{\partial t} = \frac{\partial}{\partial z} \left(\lambda \cdot \frac{\partial T}{\partial z} \right) + c_w \cdot q_{z>20}^w \cdot \frac{\partial T}{\partial z} \quad (z = 20), \quad (18)$$

$$+ (c_g \cdot q_{A-C}^g + c_w \cdot q_{A-C}^w) \cdot (T_{A-C} - T) + A_T$$

$$\frac{\partial (\rho_w \cdot S_w \cdot \phi \cdot X_{cl})}{\partial t} = \frac{\partial}{\partial z} \left(S_w \cdot \phi \cdot \frac{D_{cl}}{\theta^2} \cdot \frac{\partial (\rho_w \cdot X_{cl})}{\partial z} \right) \quad (z = 20). \quad (19)$$

$$+ q_{z>20}^w \cdot \frac{\partial X_{cl}}{\partial z} + q_{A-C}^w \cdot (X_{cl}^{A-C} - X_{cl})$$

In these equations, X_{cl}^{A-C} (mol/kg) and T_{A-C} ($^\circ\text{C}$) are the temperature and chloride concentration of the fluid laterally flowing from Zone A at 20 m bsf. Here X_{cl}^{A-C} is set to 0.613 mol/kg, which is the highest chloride concentration measured at ODP Site 1250. T_{A-C} is temperature extrapolated to 20 m bsf according to the temperatures measured at ODP Site 1250 (Figure 2f).

[39] We use the Crank-Nicolson finite difference to solve the 1D equations described above. The time step used is 0.1 year and space is discretized at 0.1 m. The parameters used are listed in Table 1.

4. Application to the Southern Summit of Hydrate Ridge

[40] Figure 4a compares dissolved chloride concentrations, calculated for $q_0^w = q_{z>20}^w = 0.5 \text{ kg}/\text{m}^2/\text{yr}$ and combinations of k values (from 0.3 to $6.0 \text{ kg}^2/\text{m}^3/\text{yr}/\text{mol}$) and simulation times (between 330 and 6400 years) that yield gas hydrate saturations above 20 m bsf of $\sim 40\%$ (Figure 4d). All the combinations produce calculated chloride-depth profiles that match the observed data. The combinations also predict the observed temperature profiles. At k values significantly above $3.0 \text{ kg}^2/\text{m}^3/\text{yr}/\text{mol}$, the rate of heat generation by hydrate crystallization produces temperatures that are too hot to be compatible with the temperature measured by

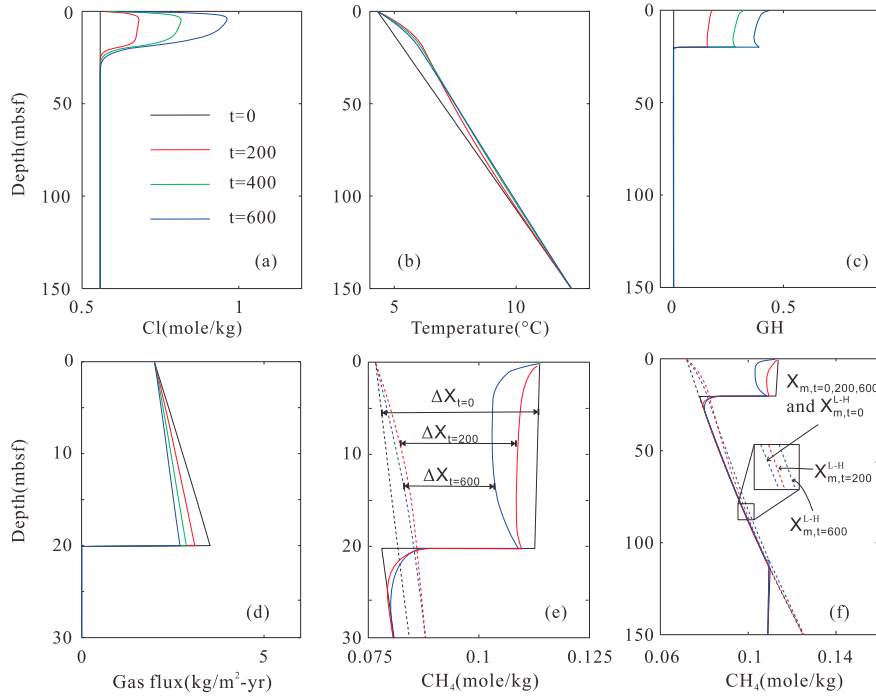


Figure 6. The changes in (a) chloride concentration, (b) temperature, (c) gas hydrate content, (d) gas flux, and driving force (e) above 20 m bsf and (f) below 20 m bsf with time at ODP 1249 for $k = 3 \text{ kg}^2/\text{m}^2/\text{yr}/\text{mol}$ at 0, 200, 400, and 600 years. Chloride concentration and gas hydrate saturation monotonically increase with time in the upper 20 m, but no obvious change occurs below ~ 20 m bsf in Figures 6a and 6c. Temperature increases rapidly at the first ~ 200 years, especially at the shallow depth, but changes little thereafter in Figure 6b. The gas flux at seafloor is set to be a constant value of $1.9 \text{ kg}/\text{m}^2/\text{yr}$ and increases downward in Figure 6d. The driving force above 20 m is the difference between X_m^{L-V} (solid lines) and X_m^{L-H-V} (dashed lines) and decreases with change in temperature and chloride concentration in Figure 6e. The driving force becomes negative below 21.5 m bsf in Figure 6f. The curves of methane concentration (solid lines) coincide below ~ 21.5 m bsf due to extremely low methane supply rate, assuming that no gas hydrate is initially present. In contrast, X_m^{L-H} (dashed lines) increases with temperature, which results in the driving force becoming negative values in Zone B, except between 20 and 21.5 m bsf where downward methane diffusion occurs.

Trehu et al. [2003]. At k values below $3.0 \text{ kg}^2/\text{m}^3/\text{yr}/\text{mol}$ (long durations of venting), the temperatures are lower than all the data points except the one at 32.5 m bsf, suggesting that the duration of venting is not more than ~ 1800 years.

[41] In order to distinguish the best fit temperature, we also calculate the sum of the absolute residuals ($A_r = \sum_{i=1}^{10} |T_i - T_s|$, where T_i is the measured temperature [Trehu et al., 2003], and T_s is the corresponding simulated temperature at the depth of T_i). The residuals are 3.28°C , 2.62°C , 1.52°C , and 3.64°C for $k = 0.3, 1.0, 3.0, 6.0 \text{ kg}^2/\text{m}^3/\text{yr}/\text{mol}$, respectively. The lowest residual for $k = 3.0 \text{ kg}^2/\text{m}^3/\text{yr}/\text{mol}$ at 650 years also best fits the measurements (black dots; Trehu et al. [2003]) as shown in Figure 4b.

[42] The methane concentration in the upper 20 m is set to a methane solubility of the liquid-vapor (L-V) system, X_m^{L-V} , and the methane concentrations evolve as shown in Figure 4c. Below 20 m bsf, the methane concentrations are almost the same. It can also be seen from Figure 4d that the hydrate accumulation is much greater above 20 m bsf (where free gas is present) than below 20 m bsf (where only dissolved methane is present and there is no free gas). The

introduction of hydrate by diffusion across the 20 m bsf horizon produces hydrate accumulation only slightly into Zone B (rounding of curves).

[43] Figure 5 shows the calculated chloride concentrations, temperature, methane concentration, and hydrate saturation profiles at ODP Site 1249 for $k = 3 \text{ kg}^2/\text{m}^3/\text{yr}/\text{mol}$ and a simulation duration of 650 years for various assigned values of surface water flux: $q_0^w = 0.5, 5, \text{ and } 50 \text{ kg}/\text{m}^2/\text{yr}$. The calculated chloride concentrations match the measured values quite well for $q_0^w = 0.5, \text{ and } 5 \text{ kg}/\text{m}^2/\text{yr}$ (Figure 5a). The calculated chloride concentrations lie below the observed range for $q_0^w = 50 \text{ kg}/\text{m}^2/\text{yr}$ because the chloride in the pore fluid is removed by the water flow faster than it is produced. The calculated temperature curves almost coincide for $q_0^w = 0.5, 5, \text{ and } 50 \text{ kg}/\text{m}^2/\text{yr}$, and the A_r values are calculated to $\sim 1.53^\circ\text{C}$, 1.52°C , and 1.59°C , respectively. The Plect number is calculated to 0.13 for the Zone C when q_0^w is set to $50 \text{ kg}/\text{m}^2/\text{yr}$. Thus, the water flux is not high enough to increase temperature and the elevation of temperature is mainly ascribed to the fast hydrate crystallization at above 20 m bsf. The calculated S_h above ~ 20 m bsf is almost identical in all cases ($\sim 40\%$, Figure 5d). We conclude that the average surface water flux,

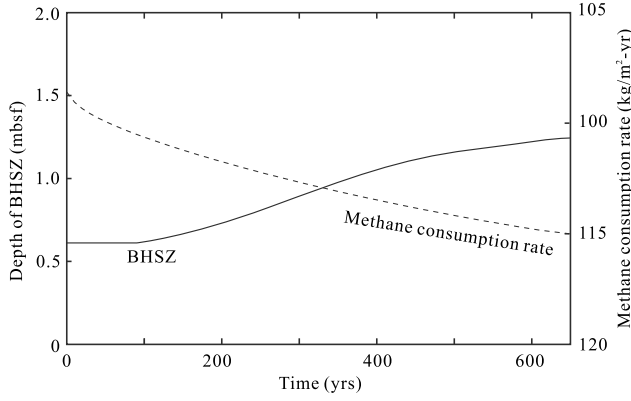


Figure 7. The BHSZ rises ~ 5 m, and the integrated methane consumption rate decreases from ~ 1.5 kg $\text{CH}_4/\text{m}^2/\text{yr}$ to ~ 0.7 kg $\text{CH}_4/\text{m}^2/\text{yr}$ as a result of the temperature and chloride concentration changes.

q_0^w , is probable ≤ 5 kg/ m^2/yr and not more than 50 kg/ m^2/yr ; otherwise, the simulated chloride would be lower than the measured values. Our calculated water flux of $q_0^w < 50$ kg/ m^2/yr is similar to the estimate of 0–2 kg/ m^2/yr from the measurements of *Torres et al.* [2002] and *Tryon et al.* [2002].

[44] Figure 6 shows how chloride concentration, temperature, hydrate saturation, gas flux, and driving force change with time for the $k = 3$ kg $^2/\text{m}^3/\text{yr}/\text{mol}$, $q_0^w = 5$ kg/ m^2/yr cases. The chloride concentration and gas hydrate saturation keep increasing (Figures 6a and 6c). The temperature increases rapidly for the first 200 years but changes very little thereafter (Figure 6b). At this point, the heat released by hydrate formation is equal to the heat loss due to thermal conduction and advection. The temperature reaches its maximum value at shallow depths at ~ 200 years. For example, at ~ 20 m bsf, the maximum temperature increase is $\sim 0.8^\circ\text{C}$ at 200 years, and thereafter the temperatures decrease slightly. At depths greater than ~ 20 m bsf, the temperature continues to slowly increase (Figure 6b). At ~ 600 years (present day in the simulations), the temperature has increased $\sim 0.2^\circ\text{C}$ at ~ 100 m bsf, which causes the BHSZ to rise from 116 m bsf to 111 m bsf (Figure 7). The increases in temperature and chloride concentration cause the driving force in the upper 20 m to decrease (Figure 6e) and cause the integrated methane consumption rate, $\int_0^{\text{BHSZ}} -R_g dz$ (kg/ m^2/yr), to decrease from 1.5 kg $\text{CH}_4/\text{m}^2/\text{yr}$ at 650 years ago to 0.7 CH_4 kg/ m^2/yr today (Figure 7). The temperature elevation in Zone B also increases methane solubility in equilibrium with the hydrate in the L-H system, requiring higher dissolved methane to form gas hydrate in Zone B. In contrast, the rate of methane supplied by diffusion and water advection is extremely low, and the calculated methane concentration changes very little in the last ~ 600 years (Figure 6f). Thus, the driving forces become increasingly negative with time below 21.5 m bsf, and gas hydrate cannot form.

5. Discussion

[45] Our calculations show that the surface water flux must be < 50 kg/ m^2/yr at the southern summit of Hydrate Ridge;

otherwise, the chloride concentration would be much lower than the measured values. The water flux of < 50 kg/ m^2/yr is too low to perturb the temperature (Figure 5b). As water advection of 50 kg/ m^2/yr has no effect on temperature, and the heat capacity of water is significantly higher than gas, the temperature would not be influenced by gas advection even if we set a gas flux to 50 kg/ m^2/yr at seafloor, which is 20 times higher than the average gas flux of 1.9 kg/ m^2/yr at the southern summit of Hydrate Ridge [*Heeschen et al.*, 2005]. *Liu and Flemings* [2006] also found that advection of heat by gas flow can be neglected, but latent heat of hydrate formation may cause significant derivation from the linear thermal gradient in a one-dimensional model at the southern summit of Hydrate Ridge. Our calculation also shows a significant temperature deviation by latent heat of hydrate formation assuming that the lateral heat loss is small compared to vertical heat loss.

[46] *Cathles et al.* [2006] derived a dimensionless vent number N_v to estimate the axial temperature changes caused by vertical heat advection in vent zones of planar or cylindrical shape. Temperature perturbations are minimal for $N_v < 0.1$. For $N_v > 2$, the temperature profile along the vent zone axis follows the 1D steady state advection profile, and horizontal heat losses are negligible. The vent number can be calculated from the ratio of the net rate of heat advected into the base of vent at time t , $q^w c_w (T_{20} - T_0)$, to twice the maximum rate of horizontal heat loss at time t , $2\pi r_v d \cdot \left(\lambda \cdot C / \sqrt{\frac{\pi \cdot \lambda}{\rho_m c_m t}} \right) \cdot [(T_{20} - T_0)/2]$ [*Cathles et al.*, 2006]. Here r_v is the radius of vent area, d is the depth of the vent hydrate system, and the calculation of C is [*Cathles et al.*, 2006]

$$\log_{10} C = 0.2734 + 0.2068\beta + 0.031\beta^2 - 0.0013\beta^3 \quad (20)$$

$$\beta = \log_{10}(t \cdot \lambda / (\rho_m c_m \cdot r_v^2)),$$

[47] The vent number for water flow at $q_0^w = 5$ kg/ m^2/yr through a 20 m thick layer with an area having a radius of $r_v = 150$ m (approximately the 300×500 m 2 area where massive gas hydrate occurs, and gas is venting at the southern Hydrate Ridge) is 0.25 for $t = 650$ years. This suggests that the water flow could warm the system very little in ~ 650 years. However, the latent heat of hydrate precipitation caused by the introduction of methane gas in the 20 m thick layer introduces heat at a rate ($\int_0^{20} A_T dz = \sim 4.7 \times 10^6$ J/ yr/m^2 at $t = 0$ and $\sim 2.2 \times 10^6$ J/ yr/m^2 at $t = 650$ years), which at 650 years is over 50 times greater than that introduced by water advection ($c_w q_0^w (T_{20} - T_0) = \sim 2.2 \times 10^4$ J/ yr/m^2 at $t = 0$ and 4.1×10^4 J/ yr/m^2 at $t = 650$ years). If this heat generation rate is substituted into the vent number expression by *Cathles et al.* [2006], the vent number ($\int_0^{20} A_T dz / \left(2 \cdot \pi \cdot r_v \cdot d \cdot \left(\lambda \cdot C / \sqrt{\frac{\pi \cdot \lambda}{\rho_m c_m t}} \right) \cdot [(T_{20} - T_0)/2] \right)$) is increased 50fold, and has a value of ~ 13.4 at $t = \sim 650$ years, which is much larger than 2.0. This indicates that we can ignore the horizontal heat loss, and our calculated temperature from one dimensional model developed here is valid for the southern summit of Hydrate Ridge.

[48] The most surprising result of the modeling is the strong contrast in accumulation time for hydrate above and below ~20 m bsf. In the gas-bearing zone above 20 m bsf, high levels of hydrate were accumulated in ~650 years, whereas in the gas-free Zone B, gas hydrate precipitation is just limited to ~1.5 m below 20 m bsf. Gas hydrate in Zone B (2%–4%) cannot form in the last ~650 years. According to *Rempel and Buffett* [1997], the rate of gas hydrate saturation increase in L-H system is

$$\frac{\partial S_h}{\partial t} = \frac{q^w \cdot \frac{\partial X_m^{L-H}}{\partial z}}{\rho_h \cdot \phi \cdot (X_m^H - X_m^{L-H})}, \quad (21)$$

where X_m^H (mol/kg) is the methane concentration in gas hydrate and $(X_m^H - X_m^{L-H}) \approx X_m^H = \frac{n_h}{M_h} = 8.2$ mol/kg. Here $\frac{\partial X_m^{L-H}}{\partial z}$ is calculated to $3.0\text{--}4.5 \times 10^{-4}$ mol/kg/m. The water flux where no active gas vent occurs is estimated to $0.9\text{--}0.1$ kg/m²/yr [Carson and Westbrook, 1995]. Thus, $\frac{\partial S_h}{\partial t}$ is between 1.0×10^{-8} and 1.0×10^{-7} yr⁻¹, and to accumulate 2%–4% of the pore volume fraction of hydrate observed there, $10^5\text{--}10^6$ years is required. However, uranium-thorium (U-Th) dating of authigenic carbonate at the southern summit of Hydrate Ridge gives ages from 800 to 6400 years and lie mainly between 1200 and 4700 years [Teichert et al., 2003]. These ages are much older than the ~650 years required to match the observed chloride and hydrate concentrations in the above ~20 m bsf but much shorter than the times required to accumulate the observed hydrate accumulations below ~20 m bsf.

[49] There are several possible explanations for this dichotomy: gas could have recently started venting, or its venting might be brief and only occasional. Comparison of seismic reflection between 2000 and 2008 also shows that the gas venting is episodic [Bangs et al., 2011]. It could also be that it vents in a much more focused fashion than the underlying regional water flux, and a particularly hydrate-rich portion of the shallow system has been sampled.

[50] Our calculation shows that hydrate can precipitate very quickly in gas-bearing zones, and its saturation can reach 30%–40% within ~650 years. Laboratory studies show that the methane gas consumption rates are about 10^4 kg/m³/yr in a short time scale from hours to days [Englezos et al., 1987a; Linga et al., 2012; Giraldo et al., 2013]. This rate is much faster than our estimated value, which might result from the differences between geological and experimental settings. Previous studies indicate that methane gas or methane-rich fluids vented ~10,000 years ago at Pinnacle (ODP Site 1250) and then diverted to the summit area as the pathways became choked with hydrate and authigenic carbonate [Milkov and Xu, 2005]. Below ~20 m bsf, the gas for hydrate formation is supplied only through biochemical production and diffusion of methane dissolved in water. To reach the 2%–4% of hydrate saturation, hydrate accumulations observed below ~20 m bsf requires between 10^5 and 10^6 years, depending on the water flux. Therefore, the gas hydrate below ~20 m bsf probably started accumulating at the southern summit of Hydrate Ridge before gas venting started there ~10,000 years ago.

6. Conclusion

[51] A 1D model is used to analyze the temperature, chloride, and hydrate depth profiles observed under a 1.0×10^5 m² area

around ODP Site 1249 at the summit of Hydrate Ridge by extrapolating the observed surface gas and water fluxes to 20 m bsf where it is assumed that gas is diverted from an adjacent locality (the Pinnacle at ODP Site 1250). The modeling analysis indicates that the observed 30% to 90% increase in pore water chlorinity, the temperature increase of ~0.8°C, and the 30% to 40% gas hydrate saturation at the summit were produced in ~650 years. For shorter venting and hydrate accumulation durations, the temperatures produced are too great, and for longer accumulation durations, the temperature increase is not great enough. The water flux at 20 m bsf is probably <5 kg/m²/yr and cannot be higher than 50 kg/m²/yr, because for higher water fluxes, the levels of chloride could not have been obtained. This water flux is similar to the preliminary estimate based on the measurements by Tryon et al. [2002] and Torres et al. [2002]

[52] The latent heat of hydrate crystallization was the main cause of the increases in temperature. The temperature increase produced a ~5 m rise in the base of the hydrate stability zone and decreased the rate of hydrate accumulation by almost 50% over the 650 years accumulation period. The 2%–4% of hydrate saturation below 20 m bsf requires between 10^5 and 10^6 years of accumulation, assuming that the water venting into the base of the hydrate stability layer was saturated with methane.

[53] The modeling suggests that hydrate accumulated rapidly under kinetic control when a stream of free methane gas was diverted to the summit area of Hydrate Ridge ~650 years ago. The rate of hydrate accumulation was reduced as temperature and chloride concentrations increased, and hydrate accumulated between the seafloor and 20 m bsf.

[54] **Acknowledgments.** This study used data provided by the Ocean Drilling Program. Funding for this study was supported by the Chinese Academy of Sciences (grant KZCX2-YW-GJ03), Chinese National Science Foundation (grant 91228206), GIGCAS 135 Program (grant Y234021001).

References

- Anderson, G. K. (2004), Enthalpy of dissociation and hydration number of methane hydrate from the Clapeyron equation, *J. Chem. Thermodyn.*, *36*, 1119–1127.
- Bangs, N. L., M. J. Hombach, and C. Berndt (2011), The mechanics of intermittent methane venting at South Hydrate Ridge inferred from 4D seismic surveying, *Earth Planet. Sci. Lett.*, *310*, 105–112.
- Bhatnagar, G., W. G. Chapman, G. R. Dickens, B. Dugan, and G. J. Hirasaki (2007), Generalization of gas hydrate distribution and saturation in marine sediments by scaling of thermodynamic and transport processes, *Am. J. Sci.*, *307*, 861–900.
- Boetius, A., and E. Suess (2004), Hydrate Ridge: a natural laboratory for the study of microbial life fueled by methane from near-surface gas hydrates, *Chem. Geol.*, *205*, 291–310.
- Bohrmann, G., E. Suess, J. Greinert, B. Teichert, and T. Naecher (2002), Gas hydrate carbonates from Hydrate Ridge, Cascadia convergent margin: indicators of near seafloor clathrate deposits, Fourth Intern. Conf. Gas Hydrates, Yokohama, Japan, 102–107.
- Carson, B., and G. K. Westbrook (1995), Modern fluid flow in the Cascadia accretionary wedge: A synthesis, *Proc. Ocean. Drill. Program Sci. Results*, *146*, 413–421.
- Cathles, L. M., and D. F. Chen (2004), A compositional kinetic model of hydrate crystallization and dissolution, *J. Geophys. Res.*, *109*, B08102, doi:10.1029/2003JB002910.
- Cathles, L. M., D. F. Chen, and B. F. Nicholson (2006), A dimensionless vent number characterizing the thermal impact of fluid discharge through planar and cylindrical vents with particular application to seafloor gas vents crystallizing hydrate, *J. Geophys. Res.*, *111*, B10205, doi:10.1029/2005JB004221.
- Chen, D. F., and L. M. Cathles (2003), A kinetic model for the pattern and amounts of hydrate precipitated from a gas steam: Application to the

- Bush Hill vent site, Green Canyon Block 185, Gulf of Mexico, *J. Geophys. Res.*, 108(B1), 2058, doi:10.1029/2001JB001597.
- Chen, D. F., L. M. Cathles (2005), On the thermal impact of gas venting and hydrate crystallization, *J. Geophys. Res.*, 110, B11204, doi:10.1029/2004JB003533.
- Chen, D. F., L. M. Cathles, and H. H. Roberts (2004), The chemical signatures of variable gas venting at hydrate sites, *Mar. Petrol. Geol.*, 21, 317–326.
- Chen, D. F., Z. Su, and L. M. Cathles (2006), Types of Gas Hydrates in Marine Environments and Their Thermodynamic Characteristics, *Terr. Atmos. Ocean. Sci.*, 17, 723–737.
- Clague, D. A., N. Maher, and C. K. Paull (2001), High-resolution multibeam survey of Hydrate Ridge, offshore Oregon, in *Natural Gas Hydrates: Occurrence, Distribution and Detection*, AGU Geophys. Monogr., vol. 124, edited by C. K. Paull and W. P. Dillon, pp. 297–303, AGU, Washington, D.C.
- Clarke, M., and P. R. Bishnoi (2000), Determination of the intrinsic rate constant of ethane gas hydrate decomposition, *Chem. Eng. Sci.*, 55, 4869–4883.
- Clarke, M., and P. R. Bishnoi (2001), Determination of the activation energy and intrinsic rate constant of methane gas hydrate decomposition, *Can. J. Civ. Eng.*, 79, 143–147.
- Colwell, F. S., S. Boyd, M. E. Delwiche, D. W. Reed, T. J. Phelps, and D. T. Newby (2008), Estimates of Biogenic Methane Production Rates in Deep Marine Sediments at Hydrate Ridge, Cascadia Margin, *Appl. Environ. Microbiol.*, 74(11), 3444–3452.
- Davie, M. K., and B. A. Buffett (2001), A numerical model for the formation of gas hydrate below the seafloor, *J. Geophys. Res.*, 106, 497–514.
- Davie, M. K., B. A. Buffett (2003a), A steady state model for marine hydrate formation: Constraints on methane supply from pore water sulfate profiles, *J. Geophys. Res.*, 108(B10), 2495, doi:10.1029/2002JB002300.
- Davie, M. K., and B. A. Buffett (2003b), Sources of methane for marine gas hydrate: inferences from a comparison of observations and numerical models, *Earth Planet. Sci. Lett.*, 206, 51–63.
- Davie, M. K., O. Y. Zatsepin, and B. A. Buffett (2004), Methane solubility in marine hydrate environments, *Mar. Geol.*, 203, 2177–184.
- Duan, Z., N. Miller, J. Greenberg, and J. Weare (1992), The prediction of methane solubility in natural waters to high ionic strengths from 0 to 250 °C and from 0 to 1600 bar, *Geochim. Cosmochim. Acta*, 56, 1451–1460.
- Englezos, P., N. Kalogerakis, P. D. Dholabhai, and P. R. Bishnoi (1987a), Kinetics of formation of methane and ethane gas hydrates, *Chem. Eng. Sci.*, 42, 2647–2658.
- Englezos, P., N. Kalogerakis, P. D. Dholabhai, and P. R. Bishnoi (1987b), Kinetics of gas hydrate formation from mixtures of methane and ethane, *Chem. Eng. Sci.*, 42, 2659–2666.
- Giraldo, C., B. Maini, R. Bishnoi, and M. Clarke (2013), A Simplified Approach to Modeling the Rate of Formation of Gas Hydrates Formed from Mixtures of Gases, *Energy Fuels*, 27(3), 1204–1211.
- Haacke, R. R., G. K. Westbrook, and R. D. Hyndman (2007), Gas hydrate, fluid flow and free gas: Formation of the bottom-simulating reflector, *Earth Planet. Sci. Lett.*, 261, 407–420.
- Haacke, R. R., G. K. Westbrook, and M. S. Riley (2008), Controls on the formation and stability of gas hydrate-related bottom-simulating reflectors (BSRs): A case study from the west Svalbard continental slope, *J. Geophys. Res.*, 113, B05104, doi:10.1029/2007JB005200.
- He, L., O. Matsubayashi, and X. Lei (2006), Methane hydrate accumulation model for the central Nankai accretionary prism, *Mar. Geol.*, 227, 201–214.
- Heeschen, K. U., A. M. Trehu, R. W. Collier, E. Suess, and G. Rehder (2003), Distribution and height of methane bubble plumes on the Cascadia Margin characterized by acoustic imaging, *Geophys. Res. Lett.*, 30(12), 1643, doi:10.1029/2003GL016974.
- Heeschen, K. U., R. W. Collier, M. A. de Angelis, E. Suess, G. Rehder, P. Linke, and G. P. Klinkhammer (2005), Methane sources, distributions, and fluxes from cold vent sites at Hydrate Ridge, Cascadia Margin, *Global Biogeochem. Cycles*, 19, GB2016, doi:10.1029/2004GB002266.
- Hyndman, R. D., and E. E. Davis (1992), A mechanism for the formation of methane hydrate and seafloor bottom-simulating reflectors by vertical fluid expulsion, *J. Geophys. Res.*, 97, 7025–7041.
- Ivanov, M., V. Blinova, E. Kozlova, G. K. Westbrook, A. Mazzini, T. Minshull, and H. Nouze (2007), First sampling of gas hydrate from the Vøring Plateau, *EOS*, 88(19), 209.
- Ivanov, M., A. Mazzini, V. Blinova, E. Kozlova, J. S. Laberg, T. Matveeva, and N. Kaskov (2010), Seep Mounds on the Southern Vøring Plateau (offshore Norway), *Mar. Petrol. Geol.*, 27, 1235–1261.
- Jerosch, K., M. Schlüter, J. P. Foucher, A. G. Allais, M. Klages, and C. Edy (2007), Spatial distribution of mud flows, chemoautotrophic communities, and biogeochemical habitats at Håkon Mosby Mud Volcano, *Mar. Geol.*, 243, 1–17.
- Johnson, H. (2011), Global resource potential of gas hydrate – a new calculation. Proceedings of the 7th International Conference on Gas Hydrates (ICGH 2011), Edinburgh, Scotland, United Kingdom, July 17–21, 2011.
- Johnson, J. E., C. Goldfinger, and E. Suess (2003), Geophysical constraints on the surface distribution of authigenic carbonates across the Hydrate Ridge region, *Mar. Geol.*, 202, 79–120.
- Kvenvolden, K. A. (1999), Potential effects of gas hydrate on human welfare, *Proc. Natl. Acad. Sci. U. S. A.*, 96, 3420–3426.
- Kvenvolden, K. A., and T. D. Lorenson (2001), The global occurrence of natural gas hydrates, in *Natural Gas Hydrates: Occurrence, Distribution and Detection*, edited by C. K. Paull and W. P. Dillon, pp. 3–18, AGU, Washington, D.C.
- Leifer, I., and I. R. MacDonald (2003), Dynamics of the gas flux from shallow gas hydrate deposits: interaction between oily hydrate bubbles and the oceanic environment, *Earth Planet. Sci. Lett.*, 21, 411–421.
- Linga, P., N. Daraboina, J. A. Ripmeester, and P. Englezos (2012), Enhanced rate of gas hydrate formation in a fixed bed column filled with sand compared to a stirred vessel, *Chem. Eng. Sci.*, 68(1), 617–623.
- Liu, X., and P. B. Flemings (2006), Passing gas through the hydrate stability zone at southern Hydrate Ridge, offshore Oregon, *Earth Planet. Sci. Lett.*, 241, 211–226.
- Liu, X., and P. B. Flemings (2007), Dynamic multiphase flow model of hydrate formation in marine sediments, *J. Geophys. Res.*, 112, B03101, doi:10.1029/2005JB004227.
- MacDonald, I. R., I. Leifer, R. Sassen, P. Stine, R. Mitchell, and N. L. Guinasso (2002), Transfer of hydrocarbons from natural seeps to the water column and atmosphere, *Geofluids*, 2, 95–107.
- MacDonald, I. R., W. W. Sager, and M. B. Peccin (2003), Gas hydrate and chemosynthetic biota in mounded bathymetry at mid-slope hydrocarbon seeps: Northern Gulf of Mexico, *Mar. Geol.*, 198, 133–158.
- Maslin, M., M. Owen, R. Betts, S. Day, T. D. Jones, and A. Ridgwell (2010), Gas hydrate: past and future geohazard?, *Phil. Trans. R. Soc. A*, 2010(368), 2369–2393.
- Matsumoto, R., M. Hiromatsu, and M. Sato (2011), Fluid flow and evolution of gas hydrate mounds of joetsu basin, eastern margin of japan sea: Constraints from high-resolution geophysical survey by AUV. Proceedings of the 7th International Conference on Gas Hydrates (ICGH 2011), Edinburgh, Scotland, United Kingdom, July 17–21, 2011.
- McConnell, D. R., Z. Zhang, and R. Boswell (2012), Review of progress in evaluating gas hydrate drilling hazards, *Mar. Petrol. Geol.*, 34(1), 209–223.
- Milkov, A. V. (2000), Worldwide distribution of submarine mud volcanoes and associated gas hydrates, *Mar. Geol.*, 167, 29–42.
- Milkov, A. V. (2005), Molecular and stable isotope composition of natural gas hydrates: A revised global dataset and basic interpretations in the context of geological settings, *Org. Geochem.*, 36(5), 681–702.
- Milkov, A. V., and W. Xu (2005), Comment on “Gas hydrate growth, methane transport, and chloride enrichment at the southern summit of Hydrate Ridge, Cascadia margin off Oregon” by Torres et al, *Earth Planet. Sci. Lett.*, 239, 162–167.
- Milkov, A. V., Y. J. Lee, W. S. Borowski, M. E. Torres, W. Xu, H. Tomaru, A. M. Trehu, P. Schultheiss, G. R. Dickens, and G. E. Claypool (2004), Co-existence of gas hydrate, free gas, and brine within the regional gas hydrate stability zone at Hydrate Ridge (Oregon margin): evidence from prolonged degassing of a pressurized core, *Earth Planet. Sci. Lett.*, 222, 829–843.
- Naudts, L., J. Greinert, J. Poort, J. Belza, E. Vangampelaere, D. Boone, P. Linke, J. Heenriet, and M. Batist (2010), Active venting sites on the gas-hydrate-bearing Hikurangi Margin, off New Zealand: Diffusive - versus bubble-released methane, *Mar. Geol.*, 272, 233–250.
- Reagan, M. T., and G. J. Moridis (2008), Dynamic response of oceanic hydrate deposits to ocean temperature change, *J. Geophys. Res.*, 113, C12023, doi:10.1029/2008JC004938.
- Reagan, M. T., G. J. Moridis, S. M. Elliott, and M. Maltrud (2011), Contribution of oceanic gas hydrate dissociation to the formation of Arctic Ocean methane plumes, *J. Geophys. Res.*, 116, C09014, doi:10.1029/2011JC007189.
- Rempel, A. W., and B. A. Buffett (1997), Formation and accumulation of gas hydrate in porous media, *J. Geophys. Res.*, 102(B5), 10,151–10,164.
- Riedel, M., T. S. Collett, and M. J. Malone, the Expedition 311 Scientists (2006a), Proc. IODP, 311: Washington, DC (Integrated Ocean Drilling Program Management International, Inc.), doi:10.2204/iodp.proc.311.2006 [Online] <http://iodp.tamu.edu/publications/exp311/311title.htm>.
- Riedel, M., I. Novosel, G. D. Spence, R. D. Hyndman, R. N. Chapman, R. C. Solem, and T. Lewis (2006b), Geophysical and geochemical signatures associated with gas hydrate-related venting in the northern Cascadia margin, *Geol. Soc. Am. Bull.*, 118(1–2), 23–38.
- Rueff, R. M., E. D. Sloan, and V. F. Yesavage (1988), Heat capacity and heat of dissociation of methane hydrates, *Am. Inst. Chem. Eng.*, 34, 1468–1476.

- Ruppel, C. D. (2011), Methane Hydrates and Contemporary Climate Change, *Nat. Educ. Knowled.*, 2(12), 12.
- Sassen, R., S. L. Losh, L. M. Cathles, H. H. Roberts, J. K. Whelan, A. V. Milkov, S. T. Sweet, and D. A. DeFreitas (2001), Massive vein-filling gas hydrate: relation to ongoing gas migration from the deep subsurface in the Gulf of Mexico, *Mar. Petrol. Geol.*, 18, 551–560.
- Sassen, R., A. V. Milkov, H. H. Roberts, S. T. Sweet, and D. A. DeFreitas (2003), Geochemical evidence of rapid hydrocarbon venting from a seafloor-piercing mud diapir, Gulf of Mexico continental shelf, *Mar. Geol.*, 198, 319–329.
- Simonetti, A., J. H. Knapp, C. C. Knapp, L. Macelloni, and C. B. Lutken (2011), Defining the hydrocarbon leakage zone and the possible accumulation model for marine gas hydrates in a salt tectonic driven cold seep: Examples from Woolsey mound, MC118, northern Gulf of Mexico. Proceedings of the 7th International Conference on Gas Hydrates (ICGH 2011), Edinburgh, Scotland, United Kingdom, July 17-21, 2011.
- Sloan, D. E., and C. A. Koh (2008), *Clathrate Hydrates of Natural Gases*, 3rd ed., CRC Press, New York.
- Suess, E., et al. (1999), Gas hydrate destabilization: enhanced dewatering, benthic material turnover and large methane plumes at the Cascadia convergent margin, *Earth Planet. Sci. Lett.*, 170, 1–15.
- Teichert, B. M. A., A. Eisenhauer, A. Haase-Schramm, B. Bock, and P. Linke (2003), U/Th systematics and ages of authigenic carbonates from Hydrate Ridge, Cascadia convergent margin: recorders of fluid composition and sea level changes, *Geochim. Cosmochim. Acta*, 67(20), 3845–3857.
- Torres, M. E., J. McManus, D. E. Hammond, M. A. de Angelis, K. U. Heeschen, S. L. Colbert, M. D. Tryon, K. M. Brown, and E. Suesse (2002), Fluid and chemical fluxes in and out of sediments hosting methane hydrate deposits on Hydrate Ridge, OR: I. Hydrological provinces, *Earth Planet. Sci. Lett.*, 201, 525–540.
- Torres, M. E., K. Wallmann, A. M. Trehu, G. Bohrmann, W. S. Borowski, and H. Tomaru (2004a), Reply to comment on: “Gas hydrate growth, methane transport and chloride enrichment at the southern summit of Hydrate Ridge, Cascadia Margin off Oregon”, *Earth Planet. Sci. Lett.*, 239, 168–175.
- Torres, M. E., K. Wallmann, A. M. Trehu, G. Bohrmann, W. S. Borowski, and H. Tomaru (2004b), Gas hydrate growth, methane transport, and chloride enrichment at the southern summit of Hydrate Ridge, Cascadia margin off Oregon, *Earth Planet. Sci. Lett.*, 226, 225–241.
- Torres M. E., J. Kim, J. Choi, B. Ryu, J. Bahk, M. Riedel, T. S. Collett, W. Hong, and M. Kastner (2011), Occurrence of high salinity fluids associated with massive near-seafloor gas hydrate deposits. Proceedings of the 7th International Conference on Gas Hydrates (ICGH 2011), Edinburgh, Scotland, United Kingdom, July 17-21, 2011.
- Trehu, A. M., G. Bohrmann, F. R. Rack and M. E. Torres (2003), Proc. ODP Init. Repts. 204.
- Trehu, A. M., et al. (2004a), Three-dimensional distribution of gas hydrate beneath southern Hydrate Ridge: Constraints from ODP Leg 204, *Earth Planet. Sci. Lett.*, 222, 845–862.
- Trehu, A. M., P. B. Flemings, N. L. Bangs, J. Chevallier, E. Gracia, J. E. Johnson, C. Liu, X. Liu, M. Riedel, and M. E. Torres (2004b), Feeding methane vents and gas hydrate deposits at south Hydrate Ridge, *Geophys. Res. Lett.*, 31, L23310, doi:10.1029/2004GL021286.
- Tryon, M. D., K. M. Brown, and M. E. Torres (2002), Fluid and chemical flux in and out of sediments hosting methane hydrate deposits on Hydrate Ridge, OR, II: hydrological processes, *Earth Planet. Sci. Lett.*, 201, 541–557.
- Whelan, J., L. Eglinton, L. Cathles, S. Losh, and H. Roberts (2005), Surface and subsurface manifestations of gas movement through a N–S transect of the Gulf of Mexico, *Mar. Petrol. Geol.*, 22(4), 479–497.
- Xu, W. (2004), Modeling dynamic marine gas hydrate systems, *Am. Min.*, 89, 1271–1279.
- Xu, W., and C. Ruppel (1999), Predicting the occurrence, distribution, and evolution of methane gas hydrate in porous marine sediments from analytical models, *J. Geophys. Res.*, 104, 5081–5096.
- Zatsepina, O. Y., and B. A. Buffett (1997), Phase equilibrium of gas hydrate: implications for the formation of hydrate in the deep sea floor, *Geophys. Res. Lett.*, 24, 1567–1570.
- Zatsepina, O. Y., and B. A. Buffett (1998), Thermodynamic conditions for the stability of gas hydrate in the seafloor, *J. Geophys. Res.*, 103(B10), 24,127–24,139.